CHEMISTRY OF MATERIALS

Article

pubs.acs.org/cm

How Does Chemistry Influence Electron Effective Mass in Oxides? A High-Throughput Computational Analysis

Geoffroy Hautier,* Anna Miglio, David Waroquiers, Gian-Marco Rignanese, and Xavier Gonze

Institute of Condensed Matter and Nanosciences, European Theoretical Spectroscopy Facility (ETSF), Université catholique de Louvain, Chemin des étoiles 8, bte L7.03.01, 1348 Louvain-la-Neuve, Belgium

ABSTRACT: Many technologies require oxides with high electronic conductivity or mobility (e.g., transparent conducting oxides, oxide photovoltaics, or photocatalysis). Using high-throughput ab initio computing, we screen more than 4000 binary and ternary oxides to identify the compounds with the lowest electron effective mass. We identify 74 promising oxides and suggest a few novel potential n-type transparent conducting oxides combining a large band gap to a low effective mass. Our analysis indicates that it is unlikely to find oxides with electron effective masses significantly lower than the current high-mobility binary oxides (e.g., ZnO and In_2O_3). Using the large data set, we extract chemical rules leading to low electron effective masses in oxides. Main group elements with $(n-1)d^{10}ns^0np^0$ cations in the rows 4 and 5 and groups 12−15 of the periodic table (i.e., Zn^{2+}, Ga^{3+}, Ge^{4+}, Cd^{2+}, In^{3+}, Sn^{4+}, and Sb^{5+}) induce the lowest electron effective masses because of their s orbitals hybridizing adequately with oxygen. More surprisingly, oxides containing 3d transition metals in a low oxidation state (e.g., Mn^{2+}) show also competitive effective masses due to the s character of their conduction band.

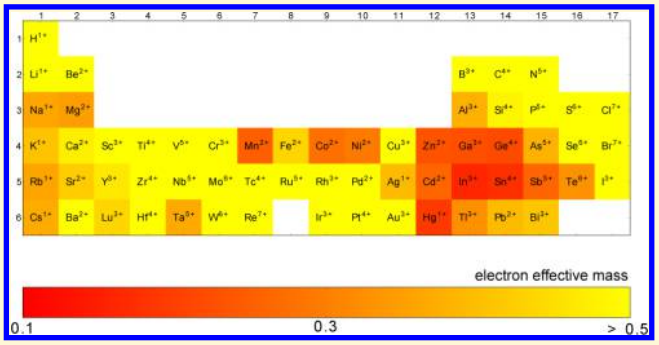

INTRODUCTION

Oxides with high carrier mobility are critical in many applications from transparent electronics to photovoltaics. By far the largest use of high-mobility oxides is to form transparent conducting oxides (TCOs) combining transparency in the visible to large electronic conductivity.[1−4] Typical TCOs are formed by a large band gap oxide doped with highly mobile (i.e., up to 100 $cm^2/(V\ s)$) carriers. n-Type TCOs are already well-developed and largely commercialized with materials such as tin-doped indium oxide (ITO) or aluminum-doped zinc oxide (AZO). However, researchers are still looking for novel n-type TCOs that would improve their fundamental properties (conductivities, mobilities, and transparency to visible light) or add application-specific properties such as stability, band alignment with other materials, work function, or etchability.[5] In addition, cost issues related, for instance, to the availability of indium have been a major driver to find novel alternative n-type TCOs. While the major field of interest for conductive oxides has been TCOs, other applications require high-mobility oxides such as all-oxide photovoltaics, oxide electronics, or photocatalysis.[6−8]

Ab initio computations have provided important insight into the properties of various conductive oxides (see, e.g., refs 9−15). In addition, high-throughput computations have recently emerged as a powerful way to rapidly search for materials with adequate properties among the large number of possible chemical compounds[16,17] in fields such as photocatalysis,[18] topological insulators,[19] Li-ion batteries,[20,21] thermoelectrics,[22,23] and lately identification of novel p-type TCO candidates with exceptionally low hole effective mass.[24]

A critical factor leading to high electronic mobility is a conduction band with a low effective mass (i.e., with a high curvature). In this work, we use a high-throughput computational approach to search for oxides with low electron effective mass. We evaluate the electron effective mass for thousands of binary and ternary oxides and systematically discuss the chemistries necessary to achieve the lowest electron effective masses. In addition, we evaluate the band gap of the most promising compounds and identify several novel potential n-type TCOs.

METHODS

Ab Initio Computations Parameters. All the high-throughput density functional theory (DFT) computations were performed using the projector augmented wave (PAW) method[25] with the generalized gradient approximation (GGA) as implemented by Perdew, Burke, and Ernzerhoff (PBE)[26] in the Vienna ab initio software package (VASP).[27] All ionic relaxations were performed using VASP with AFLOW[28] and the high-throughput computations parameters are described in Jain et al.[29]

The underestimation of the band gap is notorious in GGA for oxides with partially occupied d electrons. This can lead to a spurious metallic band structure from which by definition no effective mass can be extracted. To alleviate this issue, we computed the compounds containing an element such as V, Cr, Mn, Fe, Co, Ni, or Mo and with a GGA band gap smaller than 0.5 eV, using a Hubbard U (GGA + U).[30] We used the U advised by the Materials Project[31] to open the gap of

Received: December 12, 2013
Revised: September 6, 2014
Published: September 10, 2014

the metallic compounds. However, we must stress that this approach does not guarantee a quantitatively accurate band gap.

All computations have been performed with a ferromagnetic initialization unless otherwise specified.

More accurate band gaps can be obtained by many-body perturbation theory in the *GW* framework.[32−34] Here, we used the one-shot *GW* (or G_0W_0) approach where corrections are obtained perturbatively from a starting DFT electronic structure. *GW* and preparatory DFT calculations were performed with the ABINIT code[35] at optimized geometries, obtained from the Materials Project database. The exchange correlation energy for the preparatory DFT computation was described using the local density approximation (LDA) functional.[36] The Brillouin Zone is sampled with Monkhorst−Pack grids and the **k**-point sampling density was similar for all considered systems (>450/n **k**-points where n is the number of atoms in the unit cell). For each oxide, the planewave cutoff was determined separately and set using a total energy difference convergence criterion, leading to electronic energies converged within 10^{-3} eV on average. We used norm-conserving pseudopotentials to model the electron−ion interaction. If any, we include semicore d states as valence in the pseudopotential. The *GW* calculations were carried out using the well-established Godby-Needs plasmon-pole approximation.[37−39] We used a cutoff of 20 Ry for the expansion of the dielectric matrix and performed convergence studies with respect to the number of bands for all our candidates. The band gaps are converged within 0.1 eV (up to 1300 bands are needed).

Stability and Band Structure Analysis. The thermodynamical stability of the oxides at 0 K was analyzed using the convex hull construction. The latter effectively compares a compound energy to all linear combinations of competing phases. The construction is outlined for instance in refs 20 and 40. The stability of a compound is quantified by its energy above hull. An energy above hull of 0 meV/atom indicates a stable compound (a compound on the convex hull). The larger the energy above the hull, the less stable the phase. The stability analysis was performed using the pymatgen python package.[41]

Effective Mass Definitions. The aim of our study is to identify materials with high n-type conductivity (or electron mobility). Here, we will describe how these quantities are linked to direct properties of the band structure of the material. In an isotropic system, the conductivity (σ) is related to the concentration of electrons (n) and to their mobility (μ),

$$\sigma = ne\mu \tag{1}$$

where e is the charge of the electron.

The mobility depends on the electronic effective mass (m) and the relaxation time (τ):

$$\mu = \frac{e}{m}\tau \tag{2}$$

The relaxation time incorporates all scattering events that can influence electron conduction (impurity scattering, phonon scattering, etc.). The modeling of scattering can be very expensive computationally and will not be tackled in this high-throughput work.

On the other hand, it is relatively easy to obtain the effective mass from a simple band structure computation. For a single isotropic and parabolic conduction band, the effective mass can be obtained from the curvature of the conduction band,

$$\frac{1}{m} = \frac{1}{\hbar^2}\frac{\partial^2}{\partial k^2}E_{\text{cond}}(k_{\text{CBM}}) \tag{3}$$

where k_{CBM} is the electron wave vector corresponding to the conduction band minimum (CBM) and $E_{\text{cond}}(k)$ is the energy of the conduction band.

In general, though, the effective mass is a tensor property, the bands can be nonparabolic, and several bands and/or several pockets in different parts of the Brillouin zone can contribute to conductivity. Those complexities can be taken into account through the semiclassical Boltzmann theory assuming a constant relaxation time.[22,42] According to Boltzmann theory, the conductivity tensor is related to the band structure by

$$\sigma_{\alpha\beta} = -e^2\tau\sum_i \int \mathbf{v}_\alpha(i,\mathbf{k})\,\mathbf{v}_\beta(i,\mathbf{k})\frac{\partial}{\partial E}f(E(i,\mathbf{k}),\nu,T)\frac{\mathrm{d}\mathbf{k}}{4\pi^3} \tag{4}$$

where $E(i,\mathbf{k})$ is the energy of the ith band at the **k** wave vector, $f(E,\nu,T)$ is the Fermi−Dirac distribution with ν the chemical potential of the electron and T the temperature, and the electron speed is

$$\mathbf{v}_\alpha(i,\mathbf{k}) = \frac{1}{\hbar}\frac{\partial}{\partial \mathbf{k}_\alpha}E(i,\mathbf{k}) \tag{5}$$

Equation 4 can be simplified to the following by using an integration by part

$$\sigma_{\alpha\beta} = -e^2\tau\sum_i \int \mathbf{M}_{\alpha\beta}{}^{-1}(i,\mathbf{k})\,f(E(i,\mathbf{k}),\nu,T)\frac{\mathrm{d}\mathbf{k}}{4\pi^3} \tag{6}$$

introducing the inverse effective mass tensor at the wave vector **k** and for the ith eigenvalue ($E(i,\mathbf{k})$):

$$\mathbf{M}_{\alpha\beta}{}^{-1}(i,\mathbf{k}) = \frac{1}{\hbar^2}\frac{\partial^2}{\partial k_\alpha \partial k_\beta}E(i,\mathbf{k}) \tag{7}$$

In the case of one isotropic parabolic band, the effective mass tensor is diagonal and independent of **k** ($\mathbf{M}^{-1}(i,\mathbf{k}) = 1/m\delta_{\alpha\beta}$) and we recover the textbook expression relating conductivity to effective mass and density of carriers n:

$$\frac{\sigma_{\alpha\beta}}{\tau} = \frac{ne^2}{m}\delta_{\alpha\beta} \tag{8}$$

In the most general case, we can define an average effective mass tensor $\bar{\mathbf{M}}_{\alpha\beta}$ as

$$\bar{\mathbf{M}}_{\alpha\beta}{}^{-1} = \frac{\sigma_{\alpha\beta}}{ne^2\tau} \tag{9}$$

$$= \frac{-\sum_i \int \mathbf{M}_{\alpha\beta}{}^{-1}(i,\mathbf{k})\,f(E(i,\mathbf{k}),\nu,T)\frac{\mathrm{d}\mathbf{k}}{4\pi^3}}{\sum_i \int f(E(i,\mathbf{k}),\nu,T)\frac{\mathrm{d}\mathbf{k}}{4\pi^3}} \tag{10}$$

This average tensor $\bar{\mathbf{M}}_{\alpha\beta}$, evaluated for a chemical potential leading to a given carrier concentration (in this work 10^{18} cm^{-3}) and at the same temperature T = 300 K, can be used to compare the intrinsic tendency for materials to lead to mobile charge carriers. It takes into account nonparabolicity, anistropy, and the competitions of pockets in the Brillouin zone.

In practice, the evaluation of the average effective mass tensor through eq 10 requires a dense **k**-point sampling of the Brillouin zone (on the order of 10 000s of **k**-points), and would be time-consuming on a full database of thousands of compounds even with DFT. A useful proxy to the full average effective mass can be defined as the line effective mass:

$$m_{\text{line}} = \max_\alpha \left\{ \left[\sum_i \int -\frac{1}{\hbar^2}\frac{\partial^2}{\partial k_\alpha{}^2}E(i,\mathbf{k}_\alpha)\, f(E(i,\mathbf{k}_\alpha),\nu = E_{\text{CBM}},T = 300\text{ K})\frac{\mathrm{d}\mathbf{k}_\alpha}{\pi}\right] \Big/ \left[\sum_i \int f(E(i,\mathbf{k}_\alpha),\nu = E_{\text{CBM}},T = 300\text{ K})\frac{\mathrm{d}\mathbf{k}_\alpha}{\pi}\right]\right\} \tag{11}$$

where the maximum is taken from all the high-symmetry lines α. This line effective mass is not as accurate as determining the exact effective mass tensor but requires much less computational time (a band structure along high-symmetry lines can be obtained with only a few hundred **k**-points). Thus, it can be used as a first screening before evaluating the full average effective mass tensor.

Effective Mass Screening Approach. The workflow for our tiered screening approach is outlined in Figure 1. The first step is to evaluate the line electron effective mass for the binary and ternary

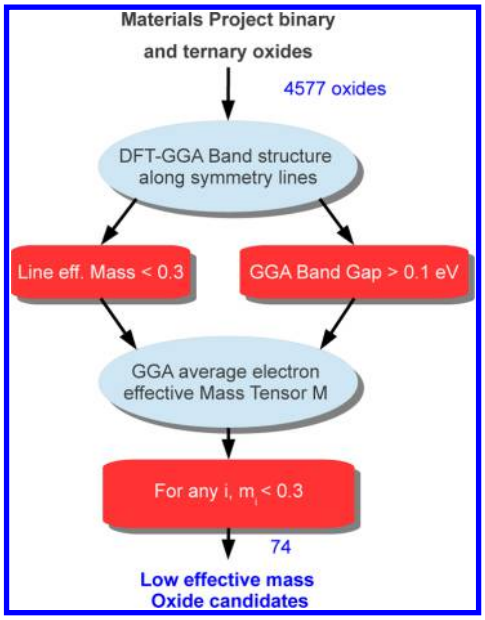

Figure 1. Flowchart for the high-throughput procedure used to search for oxides with low electron effective mass.

oxides present in the Materials Project database.[29] We used DFT with the GGA-PBE functional to compute the band structure of 4577 oxides along the high-symmetry lines defined in refs 28 and 43. We considered oxides containing less than 100 atoms in the unit cell present in the Materials Project[29,44] database and originally from the Inorganic Crystal Structure Database (ICSD).[45] Furthermore, we disregarded compounds with rare-earth elements (from Z = 58, Ce to Z = 71, Lu), inert gases, and any element with an atomic number larger than 84 (Po). For oxides containing V, Cr, Ni, Co, Mo, Fe, and Mn, we added a Hubbard U to open the gap of metallic systems. The first screening consisted of only keeping materials with a line effective mass lower than 0.3 (i.e., 2 times larger than current n-type TCOs, ZnO, SnO_2, and In_2O_3) and a GGA(+U) band gap higher than 0.1 eV. The screening on effective mass was done in two steps. First, we evaluated the line effective mass (using eq 11) and for the few compounds showing promising line effective mass, we performed a full average effective mass tensor computation through eq 10. The full average effective mass tensor computation was performed on a regular Γ-centered 8000 **k**-points grid interpolated using the Boltztrap code.[22]

RESULTS

Analysis of the Low Electron Effective Mass Oxides. *Low Electron Effective Mass Oxides Candidates.* Our study targets the identification of oxides with high electronic mobility. The electronic mobility is directly related to the electronic effective mass that can be obtained from a computed band structure (see the Methods section). We follow the tiered screening approach described in the Methods section and Figure 1 to search for oxides with very low electron effective mass among 4577 oxides. From this search, 74 oxides of interest are identified and are presented in Tables 1 and 2. We provide the three eigenvalues of the average electron effective mass tensor as well as the experimental band gaps (when available in the literature). We have separated the materials between stable (Table 1) and unstable (Table 2) compounds. We have used 50 meV/atom as a threshold to separate unstable and stable oxides.[46] The unstable materials could be metastable, high-pressure, or high-temperature phases as well as inaccurate crystal structures in the ICSD.

We should stress that our screening greatly reduced the number of possible oxides, excluding 98% of the materials in our database. Moreover, the TCOs of greatest current interest (In_2O_3, ZnO, and SnO_2) already have very low effective masses from 0.15 to 0.18. Here, we do not find any oxide with significantly lower electron effective masses and the lowest effective mass found is 0.13 for $BaSnO_3$. However, our work shows that there is a significant amount of alternative materials with effective masses between 0.15 and 0.3 and that might be of interest due to additional properties (e.g., cost, band alignment, and stability).

Previously Considered TCOs. Among the candidates, many have already been considered as TCOs. This is the case for In_2O_3, ZnO, and SnO_2 but also of the several spinel compounds of formula $CdGa_2O_4$,[56] $MgIn_2O_4$,[68] $CdIn_2O_4$,[50,71] and $ZnGa_2O_4$[70,72] and for compounds such as Ga_2O_3,[63] $InGaO_3$,[70] $ZnSnO_3$,[70] In_2TeO_6,[71] $CdSb_2O_6$,[66] and Cd_2SnO_4.[48] Our analysis also identifies $BaSnO_3$ perovskite for which high electronic mobility (up to 300 $cm^2/(V\ s)$) has been recently measured and is considered as a very promising n-type TCO.[47,73] The identification of already known or previously studied TCO materials gives us confidence in our screening approach. It justifies the focus of our study on effective mass and shows that identification of potential high-mobility oxides can be performed without modeling the detailed scattering processes.

Germanium-Based Oxides. We also find several phases never studied as TCOs and suggested computationally. A large portion of them are germanium-based compounds. Until the recent demonstration of $SrGeO_3$ as TCO,[59] germanium was not considered as an element of priority for TCO applications. Indeed, the low-pressure phase of the germanium binary oxide (GeO_2) does not show effective masses of great interest (m = 0.4−0.5). However, the GeO_2 high-pressure phase as well as several ternaries ($CdGeO_3$ polymorphs, $Cd_2Ge_7O_{16}$, $CdGe_2O_5$, Cd_2GeO_4 spinel, $ZnGeO_3$, $Zn_2Ge_3O_8$, Ga_4GeO_8, $In_2Ge_2O_7$, and Zn_2GeO_4) show attractive effective masses. Among these, only Cd_2GeO_4 has previously been studied.[62] We should note, however, that most of those phases are mixtures of Ge with an element whose binary oxide is a good TCO: Cd, Zn, In, or Ga.

Mercury-Based Oxides. Mercury-based compounds have never been considered as TCO so far. Here, we identify several mercury-containing low effective mass ternary oxides: $Hg_5Cl_2O_4$, Hg_4OF_6, $HgAs_2O_6$, and $HgAsO_3$. However, the toxicity of mercury is limiting its practical use. Toxicity is also a major issue for thallium-based compounds such as $NaTlO_2$.

Antimony-Based Oxides. Due to its electronic configuration (close to Sn^{4+}, In^{3+}, and Zn^{2+}), Sb^{5+} has been previously proposed as a promising element for TCO.[57] Our analysis reveals that several Sb-based oxides, including Sb_2O_5, show a very low effective mass. However, there is actually little literature on Sb^{5+}-based TCO materials. The experimental band gap of Sb_2O_5 has been reported around 3 eV[74,75] but recent computations with hybrid functionals cast doubt into these results by reporting a much smaller gap of 0.76 eV.[76] Among the Sb^{5+}-ternary oxides, both $NaSbO_3$ and $KSbO_3$ are reported in the ilmenite and perovskite structure (cubic or orthorhombic). The cubic perovskites show very low effective masses for both the Na and K compounds. However, there are only a few and quite old reports on the synthesis of these cubic perovskites.[77,78] It is unclear if the low effective mass cubic perovksite can be synthesized even though Shimada and Kodaira reported metastable cubic $NaSbO_3$ and $KSbO_3$.[79] Unfortunately, the more clearly established and stable $NaSbO_3$

dx.doi.org/10.1021/cm404079a | Chem. Mater. 2014, 26, 5447−5458

Table 1. Oxides with the Lowest Electron Effective Mass (<0.3)[a]

formula	space group	MP id	stability (eV/atom)	m_1	m_2	m_3	exp. band gap
$BaSnO_3$	$Pm\bar{3}m$	3163	0	0.13	0.13	0.13	3.1 eV[47]
Cd_2SnO_4	$Pmcb$	5966	0	0.15	0.14	0.13	2 eV[48]
In_2O_3	$Ia3$	22598	0	0.15	0.15	0.15	2.9 eV[12]
ZnO	$P6_3mc$	2133	0	0.15	0.15	0.15	3.4 eV[49]
$CdIn_2O_4$	$Fd\bar{3}m$	19803	0	0.16	0.16	0.16	2.67−3.24 eV[50]
$Cd_2Ge_7O_{16}$	$P\bar{4}b2$	29213	0	0.17	0.16	0.16	4.9 eV[51]
$Hg_5Cl_2O_4$	$Icma$	23358	0	0.18	0.16	0.15	
Cd_3TeO_6	$P2_1/c$	14243	0	0.18	0.17	0.16	2.8 eV,[52] 3.92 eV[53,52]
SnO_2	$P4_2/mnm$	856	0	0.18	0.18	0.16	3.6 eV[54]
In_2O_3	$R\bar{3}c$	22323	0.03	0.18	0.18	0.18	
In_6TeO_{12}	$R\bar{3}$	22189	0.01	0.18	0.18	0.18	
Hg_4OF_6	$P6_3mc$	510309	0	0.19	0.12	0.12	
$CdGeO_3$	$R\bar{3}$	8275	0.02	0.19	0.19	0.17	
$InGaO_3$	$P6_3/mmc$	22606	0	0.19	0.19	0.17	3.3 eV[55]
$ZnSnO_3$	$R3c$	13334	0.04	0.19	0.19	0.18	3.5 eV[55]
$CdGa_2O_4$	$Fd\bar{3}m$	3443	0	0.19	0.19	0.19	3.5 eV[56]
$HgAs_2O_6$	$P\bar{3}1m$	3810	0	0.2	0.18	0.18	
$Cd_2Sb_2O_7$	$Imma$	16281	0	0.2	0.18	0.18	2.7−3.5 eV[57]
$ZnSb_2O_6$	$P4_2/mnm$	3188	0	0.21	0.21	0.2	3−3.1 eV[58]
Ga_2O_3	$R\bar{3}c$	1243	0.03	0.22	0.21	0.21	
In_2TeO_6	$P321$	504908	0	0.22	0.21	0.21	
$Cd_3Cl_2O_2$	$P2_1/c$	29297	0	0.23	0.22	0.19	
$Na_2Mn_2O_3$	$P4_32_12$	566788	0	0.23	0.22	0.2	
GeO_2	$Pcnb$	10913	0.04	0.23	0.23	0.19	>4 eV[59]
Ga_2TeO_6	$P4_2/mnm$	28931	0	0.23	0.23	0.19	
$Nb_2Hg_2O_7$	$Fd\bar{3}m$	13803	0	0.23	0.23	0.21	1.8 eV[60]
$ZnGa_2O_4$	$Fd\bar{3}m$	5794	0	0.23	0.23	0.23	4.4 to 5 eV[61]
$ZnGeO_3$	$R\bar{3}$	8285	0.03	0.23	0.23	0.23	
Cd_2GeO_4	$Pcmn$	3917	0	0.24	0.22	0.2	3.15 eV[62]
Sb_2O_5	$C2/c$	1705	0	0.24	0.22	0.22	
$HgAsO_3$	$P\bar{3}1m$	30284	0	0.24	0.24	0.11	
Ga_2O_3	$C2/m$	886	0	0.24	0.24	0.22	4.9 eV[63]
In_6WO_{12}	$R\bar{3}$	25178	0.01	0.24	0.24	0.23	
InOF	$Fddd$	27175	0	0.25	0.22	0.22	
$K_2Mn_2O_3$	$P2_1/c$	19148	0	0.25	0.22	0.22	
$K_2Zn_6O_7$	$P4_2/mnm$	540728	0.01	0.25	0.23	0.21	
$In_2Ge_2O_7$	$C2/m$	5280	0	0.25	0.24	0.22	4.43 eV[64]
MnO	$Fm\bar{3}m$	19006	0	0.25	0.25	0.25	3.5 eV[65]
$NaTlO_2$	$R\bar{3}m$	3056	0	0.25	0.24	0.24	
$K_2Cd_2O_3$	$P2_1/c$	7534	0	0.26	0.22	0.2	
$CdSb_2O_6$	$P\bar{3}1m$	8922	0	0.26	0.22	0.22	4.1 eV[66]
$CdGe_2O_5$	$P\bar{1}$	7762	0.01	0.26	0.23	0.23	
Cd_3SiO_5	$P4/nmm$	13820	0	0.26	0.24	0.23	
$Ba_2In_2O_5$	$I2cm$	20546	0	0.26	0.26	0.23	
$Zn_2Ge_3O_8$	$P4_{332}$	27843	0	0.26	0.26	0.26	
$SrIn_2O_4$	$Pmnb$	540688	0	0.27	0.22	0.2	3.6 eV[67]
$Rb_2In_4O_7$	$P\bar{3}1m$	572688	0	0.27	0.24	0.24	
$Na_2Zn_2O_3$	$P2_1/c$	8086	0	0.27	0.25	0.23	
$MnGeO_3$	$R\bar{3}m$	25014	0	0.27	0.26	0.25	
Na_6MnO_4	$P6_3mc$	19321	0.02	0.27	0.25	0.25	
CoO	$Fd\bar{3}m$	19079	0.04	0.27	0.27	0.27	2.8 eV[65]
$MgIn_2O_4$	$Fd\bar{3}m$	7831	0.03	0.27	0.27	0.24	3.3 eV[68]
$KSbO_3$	$Fd\bar{3}m$	16293	0.04	0.27	0.27	0.27	
$MgSb_2O_6$	$P4_2/mnm$	3653	0	0.28	0.27	0.27	3.6 eV[19]
Sr_4I_6O	$P6_3mc$	29910	0	0.28	0.28	0.28	
Ga_4GeO_8	$C2/m$	29455	0	0.29	0.25	0.24	
$MnSb_2O_6$	$P321$	25043	0	0.29	0.25	0.25	
$Cd_2As_2O_7$	$C2/m$	10486	0.01	0.29	0.28	0.26	
Zn_2GeO_4	$R\bar{3}$	5909	0	0.29	0.29	0.27	4.1 eV[69]
Na_4I_2O	$I4/mmm$	22937	0	0.29	0.29	0.28	
$Rb_2Zn_3O_4$	$C2/c$	505501	0	0.3	0.28	0.28	

dx.doi.org/10.1021/cm404079a | Chem. Mater. 2014, 26, 5447−5458

Table 1. continued

formula	space group	MP id	stability (eV/atom)	m_1	m_2	m_3	exp. band gap
$CdGeO_3$	$C2/c$	2951	0	0.3	0.29	0.25	
$MgGa_2O_4$	$Fd\bar{3}m$	4590	0.01	0.3	0.3	0.27	

[a]Only the most stable oxides (energy above the hull <50 meV/atom) are reported here. The formula, space group, Materials Project identification (MP id), and eigenvalues of the average effective mass tensor are given. We provide the experimental band gap when found in the literature.

Table 2. Oxides with the Lowest Electron Effective Mass (<0.3)[a]

formula	space group	MP id	stability (eV/atom)	m_1	m_2	m_3
ZnO	$Fm\bar{3}m$	2229	0.15	0.17	0.17	0.17
SnO_2	$Pa3$	697	0.1	0.18	0.18	0.16
$CdGeO_3$	$Pbnm$	13003	0.12	0.18	0.18	0.17
$ScBiO_3$	$Pm\bar{3}m$	550008	0.36	0.18	0.18	0.18
Ga_2O_3	$Cmcm$	13134	0.28	0.2	0.17	0.17
$CaSnO_3$	$Pm\bar{3}m$	14113	0.19	0.21	0.21	0.21
$AlBiO_3$	$Pm\bar{3}m$	23080	0.12	0.21	0.21	0.21
$GaBiO_3$	$Pm\bar{3}m$	22979	0.23	0.22	0.22	0.22
SiO_2	$Fm\bar{3}m$	10064	1.27	0.25	0.25	0.25
Cd_2SiO_4	$Fd\bar{3}m$	560842	0.13	0.26	0.26	0.26
$NaSbO_3$	$Fd\bar{3}m$	20011	0.05	0.3	0.3	0.27
$In_2Si_2O_7$	$Fd\bar{3}m$	19784	0.13	0.3	0.3	0.28

[a]Only the least stable oxides (energy above the hull >50 meV/atom) are reported here. The formula, space group, Materials Project identification (MP id), and eigenvalues of the average effective mass tensor are given.

ilmenite and orthorhombic perovskite both have large effective masses (from 0.6 to 0.8).

We found also a series of trirutile ASb_2O_6 (A = Zn, Mg, Cd) compounds. $CdSb_2O_6$ has already been considered as TCO with an experimental gap around 4.1 eV.[66] $ZnSb_2O_6$ shows the lowest effective mass and has been studied by Kikuchi et al., indicating an encouraging conductivity (1.6×10^{-2} S cm^{-1}) and an experimental gap compatible with transparency (3−3.1 eV).[58,80] For all those compounds, the antimony orbitals play a role in the electron effective mass and the CBM has an important Sb-s character.

3d Transition-Metal-Based Oxides. It is not surprising to find only very few oxides containing elements with partially occupied d shells (e.g., Fe, Mn, Cr,...) in our low effective mass short list. The localized d character of their conduction band does not favor low effective masses. Remarkably, though, we found reasonably low effective masses for compounds with low oxidation states 3d transition metals such as Co^{2+} and Mn^{2+}. The low oxidation manganese is especially remarkable with several binary and ternary oxides with very competitive effective masses. Figure 2 shows the band structure for all Mn-based oxides with effective masses lower than 0.3: MnO, $Na_2Mn_2O_3$, $MnGeO_3$, $K_2Mn_2O_3$, Na_6MnO_4, and $MnSb_2O_6$. All of them have curvy conduction bands due to the significant Mn-s character. As oxides are often antiferromagnetic (AFM), we generated as well an AFM magnetic ordering (in the smallest supercell possible) for those compounds. Low effective masses for the condution band are still present in these AFM computations. While MnO can be disregarded as a high-mobility n-type material as it is known to present conduction by holes trapped in small polarons,[81] the Mn^{2+} ternary oxides might offer such an opportunity. Mn-based oxides could lead to materials combining high-mobility and magnetic properties. The combination of those two properties is of great interest in spintronics.

Less Stable Oxides. Table 2 refers to the more unstable compounds with low electron effective masses. High-pressure phases of the traditional TCOs such as SnO_2, ZnO, and Ga_2O_3 are present but do not show lower effective masses than the usual atmospheric pressure phases. On the other hand, many cubic perovskites show low effective masses ($AlBiO_3$, $GaBiO_3$, and $CaSnO_3$). $AlBiO_3$ and $GaBiO_3$ have not been synthesized as far as we know and both ICSD entries are from ab initio computations.[45,82] It is possible that both phases are too unstable to be synthesized. Cubic $CaSnO_3$ has only been reported by older literature according to the ICSD.[45] Interestingly, the more common rhombohedral and orthorhombic perovskites phases are more stable but unfortunately present significantly larger effective masses. This is similar to what has been described by Mizoguchi et al. for $SrGeO_3$ where only the very symmetric cubic perovskite leads to low effective mass.[59] Very low effective masses are obtained for all the $CdGeO_3$ polymorphs from ilmenite to perovskites even though the structures are quite different. Finally, the Cd_2SiO_4 spinel is found to be quite unstable. Actually, the corresponding ICSD entry links to a hypothetic structure that has only been computed and not synthesized.[45,83]

Oxides with Low Electron Effective Mass and Large Band Gap as n-Type TCO Candidates. Our screening focused on finding oxides with low electron effective mass as a necessary requirement for high electron mobility. However, for the specific TCO application, these oxides also need to be transparent to visible light. Ideally, a n-type TCO will need a band gap larger than 3 eV. We used our database to select compounds showing a very low electron effective mass (<0.25), a GGA(+U) band gap larger than 0.5 eV and a reasonable stability (energy above hull lower than 0.5 eV/atom). We also did not take into account compounds already largely studied as TCOs (e.g., ZnO, Ga_2O_3, In_2O_3, $ZnSnO_3$, $CdGa_2O_4$, and Cd_2SnO_4). For the compounds satisfying those criteria, we either relied on the experimental band gap when reported in the literature or computed it with the more accurate *GW* technique. Results for those selected few are provided in Table 3. Figure 3 shows all the computed band structures. The low effective mass due to the high curvature of the conduction band is clearly present. A few low effective mass candidates show band gaps that are definitely too small to be used as TCOs: $Cd_3Cl_2O_2$, $HgAsO_3$, $HgAs_2O_6$, $CdGeO_3$ ilmenite, In_6TeO_{12}, In_2TeO_6, and Ga_2TeO_6. $Cd_2Sb_2O_7$ has a band gap slightly lower than 3 eV and could absorb. The compounds with the most adequate gaps (>3 eV) for TCO applications are $ZnSb_2O_6$, Cd_2GeO_4, $Cd_2Ge_7O_{16}$, and GeO_2 high pressure.

Future work will be required to assess if those materials can be doped n-type and to what carrier concentration. They do not provide effective masses significantly lower than current n-type TCOs. However, other properties (e.g., stability, work function, or band alignment) might justify their use in specific applications. Unfortunately, many of them contain relatively

dx.doi.org/10.1021/cm404079a | *Chem. Mater.* 2014, 26, 5447−5458

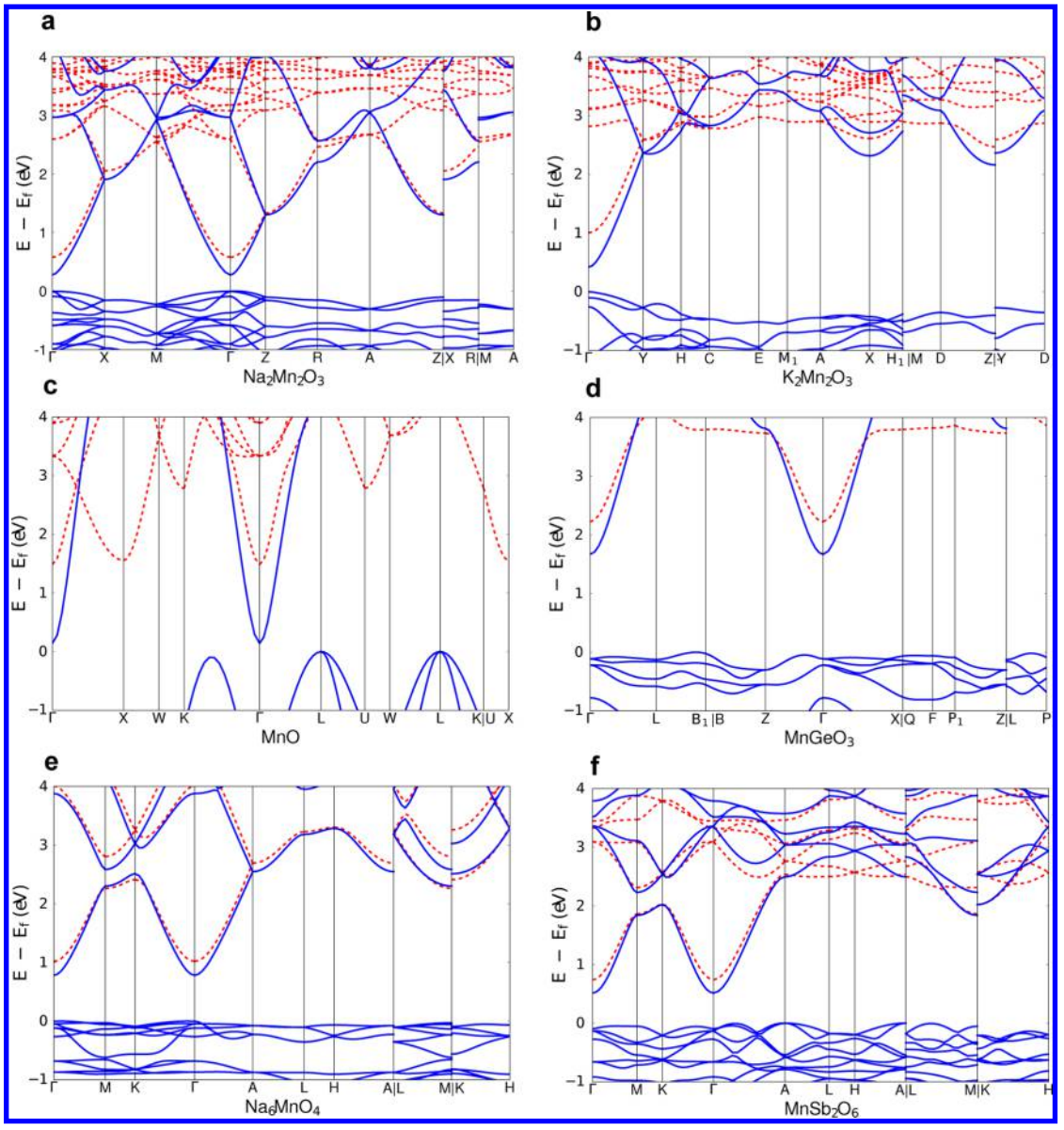

Figure 2. Band structures for the low effective mass Mn-based oxides. (a) $Na_2Mn_2O_3$, (b) $K_2Mn_2O_3$, (c) MnO, (d) $MnGeO_3$, (e) Na_6MnO_4, and (f) $MnSb_2O_6$. Spin up bands are in blue and spin down bands are in dashed red.

Table 3. Most Promising Oxides in Terms of Effective Mass with a Large Band Gap (GGA(+*U*) Band Gap Larger than 0.5 eV)[a]

formula	space group	MP id	stability (eV/atom)	m_1	m_2	m_3	band gap
$Cd_2Ge_7O_{16}$	$P\bar{4}b2$	29213	0	0.17	0.16	0.16	4.9 eV[51]
$CdGeO_3$	$R\bar{3}$	8275	0.02	0.19	0.19	0.17	2.4 eV (*GW*)
$Cd_2Sb_2O_7$	*Imma*	16281	0	0.2	0.18	0.18	2.7[57]
$HgAs_2O_6$	$P\bar{3}1m$	3810	0	0.2	0.18	0.18	1 eV (*GW*)
$ZnSb_2O_6$	$P4_2/mnm$	27843	0	0.21	0.21	0.2	3−3.1 eV[58]
GeO_2	*Pcnb*	10913	0.04	0.23	0.23	0.19	>4 eV[59]
$Cd_3Cl_2O_2$	$P2_1/c$	29297	0	0.23	0.22	0.19	1.7 eV (*GW*)
Cd_2GeO4	*Pcmn*	3917	0	0.24	0.22	0.2	3.15[62]
$HgAsO_3$	$P\bar{3}1m$	30284	0	0.24	0.24	0.11	2.4 eV (*GW*)
In_6TeO_{12}	$R\bar{3}$	22189	0.01	0.18	0.18	0.18	1.7 eV (*GW*)
In_2TeO_6	*P*321	504908	0	0.22	0.21	0.21	2.0 eV (*GW*)
Ga_2TeO_6	$P4_2/mnm$	28931	0	0.23	0.23	0.19	2.2 eV (*GW*)

[a]The formula, space group, Materials Project identification (MP id), and eigenvalues of the average effective mass tensor are given. For all oxides, we either reported the experimentally measured or *GW*-computed band gap.

dx.doi.org/10.1021/cm404079a | *Chem. Mater.* 2014, 26, 5447−5458

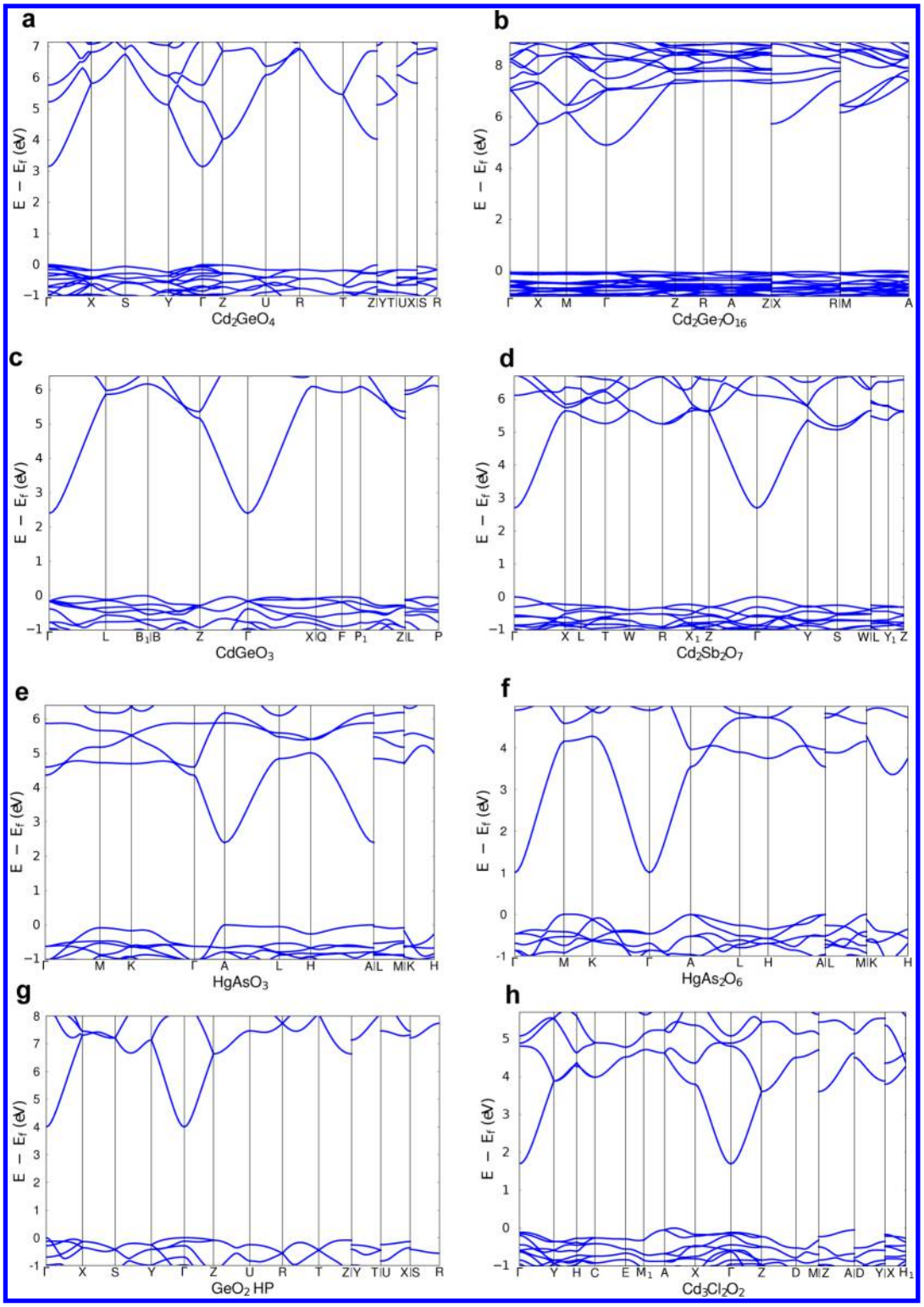

Figure 3. Band structures of the low electron effective mass n-type TCO candidates. (a) Cd_2GeO_4, (b) $Cd_2Ge_7O_{16}$, (c) $CdGeO_3$, (d) $Cd_2Sb_2O_7$, (e) $HgAsO_3$, (f) $HgAs_2O_6$, (g) GeO_2 HP, and (h) $Cd_3Cl_2O_2$. All band structures are from GGA with a scissor shift of the conduction band to fit the *GW* or experimentally measured band gap value.

rare or toxic elements (e.g., Cd, Te, In, Hg, or Ge), with the only notable exception being $ZnSb_2O_6$.

Chemical Analysis of Low Effective Mass Oxides. Our large database of band structures provides a data set of interest for discovering the chemical reasons for low electronic effective masses in oxides. Knowing the ingredients necessary for low electron effective masses will facilitate the future search for high electronic mobility oxides. The effective mass is mainly determined by the band structure close to the CBM and the chemical nature of the CBM is accessible by studying the projection of the wave function at the CBM on different elements and orbitals (s, p, or d). Here, we look at correlations

dx.doi.org/10.1021/cm404079a | *Chem. Mater.* 2014, 26, 5447−5458

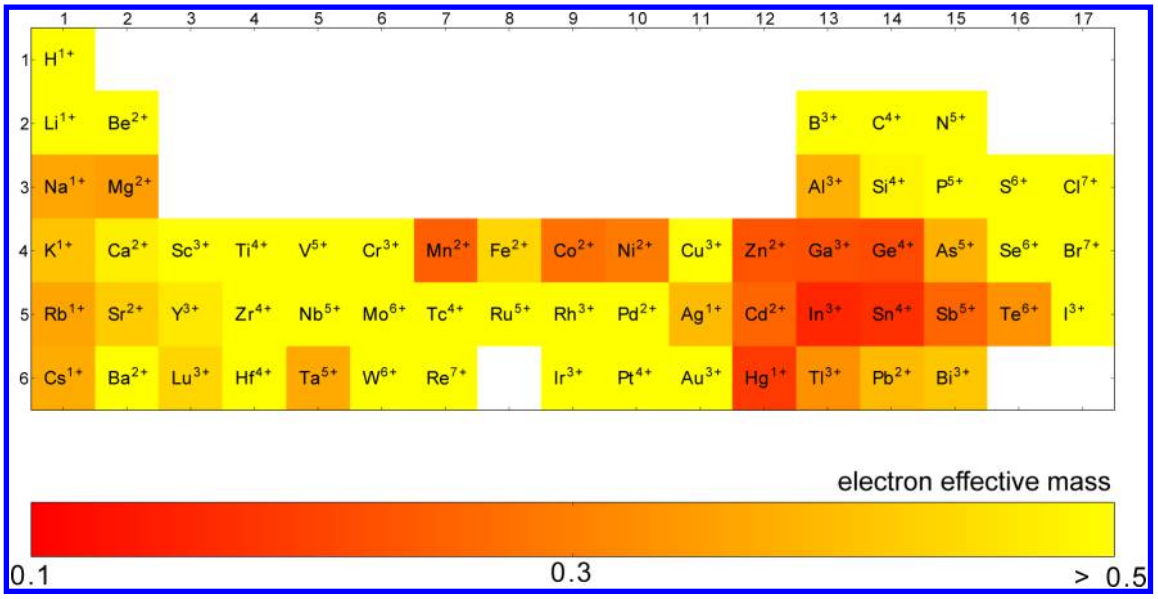

Figure 4. Lowest electron effective mass for each cation plotted in rows and columns of the periodic table. We considered only oxides (binaries or ternaries) with a clear majority of a given cation in the CBM nature (higher than 80%). This unambigously leads to attributing the effective mass value to a specific metal character. The printed ion indicates in what oxidation state the metallic element is (according to the ICSD).

between the value of the effective mass and the CBM character. To simplify the analysis, we considered only compounds having oxygen as the only anion (i.e., we have not taken into account oxychlorides or oxyfluorides, for instance).

The nature of the conduction band in TCOs has already been debated in the literature. First theories considered a purely cationic character of the conduction band and a band curvature determined by cation−cation overlap. More recently, several computational results have demonstrated that TCOs have a significant oxygen character in their conduction band.[11,57,59,84,85] Our data set is consistent with this view and the majority of oxides (70%) have at least 5% oxygen character at the CBM. When a simple tight-binding picture is followed, the effective mass is mainly determined by the cation to oxygen overlap at the CBM.[84,86] The nature of the cation hybridizing with oxygen should then be critical to obtaining low effective masses.

We studied what cationic character of the CBM leads to the lowest electron effective masses. To simplify the problem, we considered only oxides (binaries or ternaries) with a clear majority of a given cation in the CBM nature (higher than 80%). This unambiguously leads to attributing the effective mass value to a specific metal character. For this subset of compounds, we also attributed an oxidation state to the metal forming the CBM by using the oxidation state provided in the ICSD. This procedure allows us to identify the exact cation (element and oxidation state) responsible for a low or high effective mass. For instance, in the case of $Na_2Zn_2O_3$, this analysis shows that the CBM is mostly of Zn^{2+} nature and the Na^+ cation does not directly influence the effective mass.

We plotted in Figure 4 the *lowest* electron effective mass obtained for each element. The data has been organized by rows and columns of the periodic table to study the influence of the electronic configuration on the effective mass. For each element, we have printed the cation in the lowest electron effective mass oxide. A region of very low effective mass is observed between group 12 and group 15 in rows 4 and 5 (Zn^{2+}, Ga^{3+}, Ge^{4+}, Cd^{2+}, In^{3+}, Sn^{4+}, and Sb^{5+}) as well as for some 3d reduced transition metals (Mn^{2+}, Co^{2+}, and Ni^{2+}).

The character (s, p, or d) of the cationic orbital should strongly influence the orbital overlap. Figure 5 shows the s, p, or d character for the CBM of each lowest electron effective mass oxide. In a comparison of Figure 4 to Figure 5, the lowest effective masses chemistries are correlated with a strong s character in the CBM. On the other hand, compounds with large d character at the CBM have much larger electronic effective mass. Interestingly, for some of the low oxidation states 3d transition metals (i.e., Mn^{2+}, Co^{2+}, Ni^{2+}, and Fe^{2+}) the CBM can have a strong s character and therefore low effective masses. This is in agreement with recent hybrid functional computations on binary transition-metal oxides.[87] The 3d transition metals have an electronic configuration of $(n-1)d^x ns^2$ with x between 3 (for V) and 10 (for Cu) and only low oxidation states (+1 or +2) can lead to an s character for the conduction band. Mn^{2+} is of greatest interest in view of several ternary oxides exhibiting low electronic effective masses.

Among compounds with a high d character for their CBM, we identify $AgTaO_3$ rhombohedral perovskite to have the lowest electron effective mass. The Ta-d character of the conduction band of $AgTaO_3$ is in agreement with Kato et al.[88] Full average effective mass tensor indicates effective mass eigenvalues of 0.44, 0.48, and 0.48, which is low for d-electron-based compounds but still 2 times larger than the effective masses obtained with CBMs of s character.

An important s character of the CBM is necessary to reach low effective masses but it is not sufficient. Cations inducing large s character such as the alkali (Na^+, Li^+, Cs^+, and Rb^+) and some main group cations (Al^{3+}, Te^{6+}, and Se^{6+}) do not lead to effective masses as low as Sn^{4+}, Zn^{2+}, etc. This indicates that in addition to an s character, the cation orbital needs to be at an adequate energy level to hybridize with oxygen. The optimal hybridization appears for a region of the main group elements between columns 12 and 15 and rows 4 and 6 (Zn^{2+}, Ga^{3+}, Ge^{4+}, Cd^{2+}, In^{3+}, Sn^{4+}, and Sb^{5+}), as well as for some reduced 3d metals (e.g., Mn^{2+}).

The low electron effective mass induced by $(n-1)d^{10}ns^0np^0$ cations is in agreement with what has been observed in the field of TCOs (see, for instance, Hoel et al.[89]) with the exception of

dx.doi.org/10.1021/cm404079a | *Chem. Mater.* 2014, 26, 5447−5458

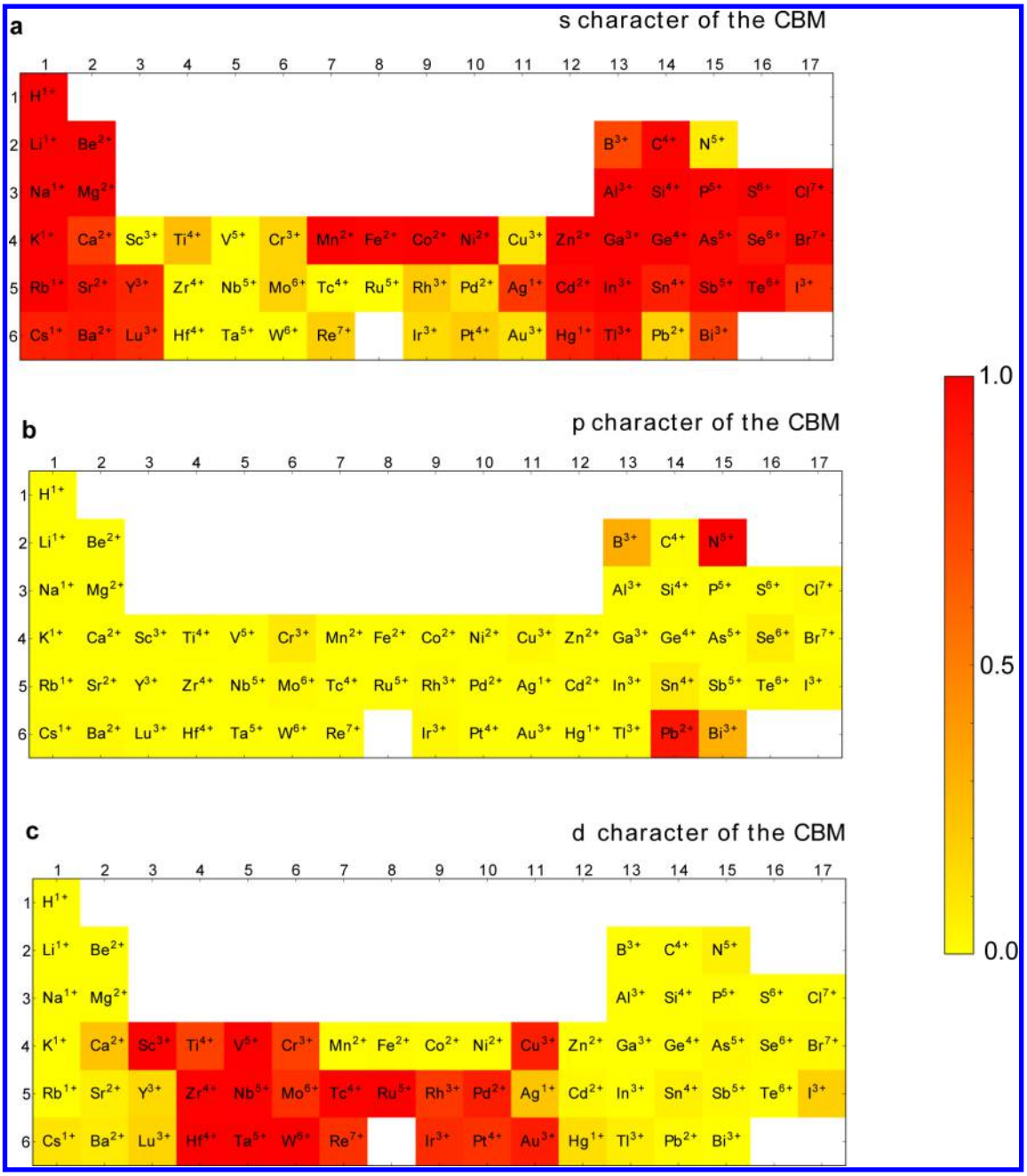

Figure 5. Orbital character (s, p, or d) of the CBM for the lowest effective mass oxides for each cation plotted in rows and columns of the periodic table. We considered only oxides (binaries or ternaries) with a clear majority of a given cation in the CBM nature (higher than 80%). This unambigously leads to attributing the effective mass value to a specific metal character. The printed ion indicates in what oxidation state the metallic element is (according to the ICSD).

Ge^{4+} which has not been traditionally considered for TCO applications. On the other hand, the finding that the +2 transition metals (e.g., Mn^{2+}) can also lead to low electron effective mass materials by using the s character of their CBM is more surprising.

We should stress that we assumed oxygen to be the only anion. When an additional anion is present, our conclusions are not valid anymore. For instance, Sr_4I_6O and Na_4I_2O show lower effective masses than pure Sr- and Na-based oxides (see Table 1)

Finally, the presence of specific cations is a necessary but not sufficient condition to obtain low electronic effective mass. Indeed, the crystal structure needs to also favor orbital overlap and other elements present should not influence the conduction band character. For instance, $In_2Te_3O_9$ (MP id: 560509) and $Zn_3As_2O_6$ (MP id: 27580) contain both In^{3+} and Zn^{2+} (ions that can lead to low effective masses) but the third element (Te or As) plays a role in the conduction band character and leads to high effective masses (respectively (17.1, 4.2, 1.6) and (4.1, 1.6, 0.9) as eigenvalues of the average effective mass tensor).

■ DISCUSSION AND CONCLUSIONS

Oxides with high electron mobility are essential to many applications including n-type TCOs, electronics, and photocatalysis. Using high-throughput computing, we have searched

dx.doi.org/10.1021/cm404079a | *Chem. Mater.* 2014, 26, 5447−5458

for oxides with low electron effective masses among 4577 oxides. We identify oxides that have never been looked at as conductive oxides before. The analysis of our database has helped outline the chemical rules necessary for low electron effective mass.

The starting computational approach we used is DFT. Indeed, effective masses and bandwidths are usually well-reproduced by the DFT-GGA functionals (see, for instance, Dixit et al.[61]). Actually, effective masses tend to be underestimated but in a systematic way, making them very useful to screen for the lowest effective mass materials. On the other hand, the GGA band gaps are always strongly underestimated and with a large error spread.[90] The more accurate G_0W_0 technique that we used for some oxides improves this band gap but nevertheless still tends to underestimate it.[34] The underestimation is usually around 0.2 eV on average but can be much higher (up to 0.8 eV in the exceptional case of ZnO[38]).

The most straightforward implication of our work is to identify potential novel n-type TCOs. By identifying oxides with low electron effective mass and large band gaps, we found materials satisfying two necessary but not sufficient properties of a good TCO. Indeed, an n-type TCO would require satisfying other constraints such as n-type dopability. Follow-up defect studies will be required on the few candidates with low effective masses and large band gaps.

Our study demonstrates that it will be difficult to dramatically surpass the current n-type TCOs (e.g., ZnO, SnO_2, and In_2O_3) in terms of effective masses as they are already among the lowest that can be found in oxides. A strategy to significantly improve the n-type mobilities compared to current n-type TCOs will be to target materials with low effective masses (e.g., some of the oxides presented in this work) but to engineer the remaining factor involved in mobility which is the scattering time. This might be what is at play in the extremely high mobilities reported recently for $BaSnO_3$.[47]

In any case, a new n-type TCO does not require having significantly larger mobilities and conductivities than current technologies. Such a new material could be of interest if it keeps effective masses (and mobilities) close to known n-type TCOs but performs better on additional application-specific properties (e.g., work function, band offsets, cost, or stability). By filtering among the thousands of chemical possibilities to select only the most promising compounds, we have shown that our study provides a set of good candidates (e.g., Cd_2GeO_4, $Cd_2Ge_7O_{16}$, and $ZnSb_2O_6$) for further computational and experimental studies. We should stress that even materials that have already been studied as conducting oxides (e.g., $ZnSb_2O_6$[58]) could benefit from a reinvestigation. Indeed, process conditions can be critical to unleash a TCO full potential. In the case of $BaSnO_3$, the first experimental results showed a 2 $cm^2/(V\ s)$ mobility when the recent more optimized results report an impressive 300 $cm^2/(V\ s)$.[47]

Using our large database, we have been able to establish on a firm footing which chemistries promote the formation of low electron effective mass oxides. Those rules will be of great use for the field of n-type TCOs in other fields such as oxide photovoltaics, photocatalysis, or oxide electronics where high mobility is also sought for. The chemistries we discovered are based on main group $(n-1)d^{10}ns^0np^0$ ions (with n = 4, 5) such as Zn^{2+}, Sn^{4+}, and Cd^{2+}, which offer s orbitals with optimal hybridization with the oxygen orbitals and lead to very low effective masses. Among the cations of interest, we also found in our study that Ge^{4+}, which has been only recently presented as a potential n-type TCO cation,[59] is less exceptional than expected and that many ternary oxides containing Ge form low electron effective mass materials.

We also show that combining magnetic elements with low electronic effective mass might be achievable using Co^{2+}, Ni^{2+}, or Fe^{2+} but more importantly Mn^{2+}-based compounds. The s orbital character induced at the CBM level by the presence of Mn^{2+} can lead to competitive effective masses in MnO but also ternary oxides (e.g., $MnGeO_3$ and $K_2Mn_2O_3$). This finding is very exciting for the development of new materials combining magnetism and high mobility, which could be of great use in spintronics.

We confirm that it will be difficult to avoid the use of the rows 4 through 5 main group elements without compromising the effective mass and to use instead alkali-earth or Al-based oxides as they will suffer from inherently higher effective masses. This is in agreement with previous results from Medvedva on a smaller set of compounds.[84]

Finally, while the main approach to n-type ternary TCOs has been to mix two good binary TCOs (e.g., ZnO and SnO_2 in $ZnSnO_3$ and refs 55, 70, and 89), our study shows that this is not necessary. We find several compounds with low effective mass and resulting from the mixing of an element known to give good mobilities in the binary with another element (not associated with good TCO properties). This design idea had already been used in p-type TCOs where Cu, Ag, or Sn (known to form relatively good binary p-type oxides) are mixed with another element.[24,91−93] Here, we find low effective masses for the In-based (In_6WO_{12}, InOF, $Ba_2In_2O_5$, $Rb_2In_4O_7$, $SrIn_2O_4$, and $In_2Si_2O_7$), the Ga-based ($MgGa_2O_4$), the Cd-based ($Cd_3Cl_2O_2$, Cd_3SiO_5, Cd_2SiO_4, and $Cd_2As_2O_7$), and the Zn-based ($K_2Zn_6O_7$, $Na_2Zn_2O_3$, and $Rb_2Zn_3O_4$). In those ternary oxides, only one of the elements induces the low effective mass as the others are not present in the character of the conduction band. This conclusion offers great opportunities to extend the chemical space of ternary TCOs. We hope this systematic high-throughput analysis will help future materials design of n-type TCOs as well as oxides for electronics, photovoltaics, and photocatalysis.

AUTHOR INFORMATION

Corresponding Author

*E-mail: geoffroy.hautier@uclouvain.be.

Notes

The authors declare no competing financial interest.

ACKNOWLEDGMENTS

Geoffroy Hautier and Gian-Marco Rignanese acknowledge the F.R.S.-FNRS for financial support. The work was supported by the European Union Marie Curie Career Integration (CIG) grant HTforTCOs PCIG11-GA-2012-321988. The authors acknowledge technical support and scientific advice from J.-M. Beuken and M. Giantomassi. This work was also supported by the Agentschap voor Innovatie door Wetenschap en Technologie (IWT project no. 080023, ISIMADE) and the FRS-FNRS through FRFC project 2.4.589.09.F. Computational resources have been provided by the supercomputing facilities of the Université catholique de Louvain (CISM/UCL) and the Consortium des Équipements de Calcul Intensif en Fédération Wallonie Bruxelles (CÉCI) funded by the Fond de la Recherche Scientifique de Belgique (FRS-FNRS).

REFERENCES

(1) Ellmer, K. *Nat. Photonics* **2012**, *6*, 809−817.
(2) Ginley, D. S.; Hosono, H.; Paine, D. C. *Handbook of Transparent Conductors*; Springer: New York, 2010
(3) Ginley, D. S.; Bright, C. *MRS Bull.* **2000**, *25*, 15−18.
(4) Granqvist, C. G. *Sol. Energy Mater. Sol. Cells* **2007**, *91*, 1529−1598.
(5) Gordon, R. *MRS Bull.* **2000**, *25*, 52−57.
(6) Rühle, S.; Anderson, A. Y.; Barad, H.-N.; Kupfer, B.; Bouhadana, Y.; Rosh-Hodesh, E.; Zaban, A. *J. Phys. Chem. Lett.* **2012**, *3*, 3755−3764.
(7) Fortunato, E.; Barquinha, P.; Martins, R. *Adv. Mater.* **2012**, *24*, 2945−2986.
(8) Liao, P.; Carter, E. A. *Chem. Soc. Rev.* **2013**, *42*, 2401−2422.
(9) Lany, S.; Zunger, A. *Phys. Rev. Lett.* **2007**, *98*, 2−5.
(10) Scanlon, D. O.; Watson, G. W. *J. Phys. Chem. Lett.* **2010**, *1*, 3195−3199.
(11) Medvedeva, J. E.; Hettiarachchi, C. L. *Phys. Rev. B* **2010**, *81*, 1−16.
(12) Walsh, A.; Da Silva, J.; Wei, S.-H.; Körber, C.; Klein, A.; Piper, L.; DeMasi, A.; Smith, K.; Panaccione, G.; Torelli, P.; Payne, D.; Bourlange, A.; Egdell, R. *Phys. Rev. Lett.* **2008**, *100*, 167402.
(13) Walsh, A.; Da Silva, J. L. F.; Wei, S.-H. *J. Phys.: Condens. Matter* **2011**, *23*, 334210.
(14) Varley, J.; Janotti, A.; Franchini, C.; Van de Walle, C. *Phys. Rev. B* **2012**, *85*, 2−5.
(15) Hoffling, B.; Schleife, A.; Fuchs, F.; Rodl, C.; Bechstedt, F. *Appl. Phys. Lett.* **2010**, *97*, 032116.
(16) Hautier, G.; Jain, A.; Ong, S. P. *J. Mater. Sci.* **2012**, *47*, 7317−7340.
(17) Curtarolo, S.; Hart, G. L. W.; Nardelli, M. B.; Mingo, N.; Sanvito, S.; Levy, O. *Nat. Mater.* **2013**, *12*, 191−201.
(18) Wu, Y.; Lazic, P.; Hautier, G.; Persson, K.; Ceder, G. *Energy Environ. Sci.* **2013**, *6*, 157.
(19) Yang, K.; Setyawan, W.; Wang, S.; Buongiorno Nardelli, M.; Curtarolo, S. *Nat. Mater.* **2012**, *11*, 614−619.
(20) Chen, H.; Hautier, G.; Jain, A.; Moore, C.; Kang, B.; Doe, R.; Wu, L.; Zhu, Y.; Tang, Y.; Ceder, G. *Chem. Mater.* **2012**, *24*, 2009−2016.
(21) Hautier, G.; Jain, A.; Ong, S. P.; Kang, B.; Moore, C.; Doe, R.; Ceder, G. *Chem. Mater.* **2011**, *23*, 3945−3508.
(22) Madsen, G. K. H. *J. Am. Chem. Soc.* **2006**, *128*, 12140−12146.
(23) Wang, S.; Wang, Z.; Setyawan, W.; Mingo, N.; Curtarolo, S. *Phys. Rev. X* **2011**, *1*, 1−8.
(24) Hautier, G.; Miglio, A.; Ceder, G.; Rignanese, G.-M.; Gonze, X. *Nat. Commun.* **2013**, *4*, 2292.
(25) Blöchl, P. *Phys. Rev. B* **1994**, *50*, 17953−17979.
(26) Perdew, J.; Burke, K.; Ernzerhof, M. *Phys. Rev. Lett.* **1996**, *77*, 3865−3868.
(27) Kresse, G.; Furthmuller, J. *Comput. Mater. Sci.* **1996**, *6*, 15−50.
(28) Curtarolo, S.; Setyawan, W.; Wang, S.; Xue, J.; Yang, K.; Taylor, R. H.; Nelson, L. J.; Hart, G. L.; Sanvito, S.; Buongiorno-Nardelli, M.; Mingo, N.; Levy, O. *Comput. Mater. Sci.* **2012**, *58*, 227−235.
(29) Jain, A.; Hautier, G.; Moore, C. J.; Ong, S. P.; Fischer, C. C.; Mueller, T.; Persson, K. A.; Ceder, G. *Comput. Mater. Sci.* **2011**, *50*, 2295−2310.
(30) Dudarev, S. L.; Savrasov, S. Y.; Humphreys, C. J.; Sutton, A. P. *Phys. Rev. B* **1998**, *57*, 1505−1509.
(31) *The Materials Project wiki;* http://materialsproject.org/wiki/index.php/GGA%2BU_calculations (accessed September 24, 2014).
(32) Hybertsen, M. S.; Louie, S. G. *Phys. Rev. B* **1986**, 5390.
(33) Friedrich, C.; Schindlmayr, A. In *Computational Nanoscience: Do It Yourself!*; Grotendorst, J., Blügel, S., Marx, D., Eds.; John von Neumann Institute for Computing: Jülich, Germany, 2006; Vol. *31*, pp 335−355.
(34) van Schilfgaarde, M.; Kotani, T.; Faleev, S. *Phys. Rev. Lett.* **2006**, *96*, 226402.
(35) Gonze, X.; Amadon, B.; Anglade, P.-M.; Beuken, J.-M.; Bottin, F.; Boulanger, P.; Bruneval, F.; Caliste, D.; Caracas, R.; Côté, M.; Deutsch, T.; Genovese, L.; Ghosez, Ph.; Giantomassi, M.; Goedecker, S.; Hamann, D. R.; Hermet, P.; Jollet, F.; Jomard, G.; Leroux, S.; Mancini, M.; Mazevet, S.; Oliveira, M. J. T.; Onida, G.; Pouillon, Y.; Rangel, T.; Rignanese, G.-M.; Sangalli, D.; Shaltaf, R.; Torrent, M.; Verstraete, M. J.; Zerah, G.; Zwanziger, J. W. *Comput. Phys. Commun.* **2009**, *180*, 2582−2615.
(36) Perdew, J.; Wang, Y. *Phys. Rev. B* **1992**, *45*, 244−249.
(37) Godby, R.; Needs, R. *Phys. Rev. Lett.* **1989**, *62*, 1169−1172.
(38) Stankovski, M.; Antonius, G.; Waroquiers, D.; Miglio, A.; Dixit, H.; Sankaran, K.; Giantomassi, M.; Gonze, X.; Côté, M.; Rignanese, G.-M. *Phys. Rev. B* **2011**, *84*, 241201.
(39) Miglio, A.; Waroquiers, D.; Antonius, G.; Giantomassi, M.; Stankovski, M.; Côté, M.; Gonze, X.; Rignanese, G. M. *Eur. Phys. J. B* **2012**, *85*, 322.
(40) Ong, S. P.; Wang, L.; Kang, B.; Ceder, G. *Chem. Mater.* **2008**, *20*, 1798−1807.
(41) Ong, S. P.; Richards, W. D.; Jain, A.; Hautier, G.; Kocher, M.; Cholia, S.; Gunter, D.; Chevrier, V. L.; Persson, K. A.; Ceder, G. *Comput. Mater. Sci.* **2013**, *68*, 314−319.
(42) Ashcroft, N. W.; Mermin, N. D. *Solid State Physics*; Thomson Learning: London, 1976; p 848.
(43) Setyawan, W.; Curtarolo, S. *Comput. Mater. Sci.* **2010**, *49*, 299−312.
(44) *The Materials Project;* http://www.materialsproject.org (accessed September 1, 2013).
(45) *ICSD, Inorganic Crystal Structure Database*; http://www.fiz-karlsruhe.de/icsd.html; FIZ Karlsruhe: Karlsruhe, Germany, 2013.
(46) Hautier, G.; Ong, S. P.; Jain, A.; Moore, C. J.; Ceder, G. *Phys. Rev. B* **2012**, *85*, 155208.
(47) Kim, H. J.; Kim, U.; Kim, H. M.; Kim, T. H.; Mun, H. S.; Jeon, B.-G.; Hong, K. T.; Lee, W.-J.; Ju, C.; Kim, K. H.; Char, K. *Appl. Phys. Express* **2012**, *5*, 061102.
(48) Nozik, A. J. *Phys. Rev. B* **1972**, *6*, 453.
(49) Reynolds, D.; Look, D.; Jogai, B.; Litton, C.; Cantwell, G.; Harsch, W. *Phys. Rev. B* **1999**, *60*, 2340−2344.
(50) Pisarkiewicz, T.; Zakrezewska, K.; Leja, E. *Thin Solid Films* **1987**, *153*, 479−486.
(51) Che, G.; Li, X.; Liu, C.; Wang, H.; Liu, Y.; Xu, Z. *Phys. Status Solidi* **2008**, *205*, 194−198.
(52) Tetsuka, H.; Shan, Y. *J. Mater. Res.* **2005**, *20*, 2−6.
(53) Tetsuka, H.; Shan, Y. J.; Tezuka, K.; Imoto, H. *Solid State Commun.* **2006**, *137*, 345−349.
(54) Reimann, K.; Steube, M.; Dortmund, U. *Solid State Commun.* **1998**, *105*, 649−652.
(55) Minami, T. *J. Vac. Sci. Technol., A* **1999**, *17*, 1765.
(56) Omata, T.; Ueda, N.; Hikuma, N.; Ueda, K.; Mizoguchi, H.; Hashimoto, T.; Kawazoe, H. *Appl. Phys. Lett.* **1993**, *62*, 499.
(57) Mizoguchi, H.; Eng, H. W.; Woodward, P. M. *Inorg. Chem.* **2004**, *43*, 1667−1680.
(58) Kikuchi, N.; Hosono, H.; Kawazoe, H.; Tanegashima, O.; Ota, I.; Kimura, Y. *J. Am. Ceram. Soc.* **2005**, *88*, 2793−2797.
(59) Mizoguchi, H.; Kamiya, T.; Matsuishi, S.; Hosono, H. *Nat. Commun.* **2011**, *2*, 470.
(60) Kung, H. H.; Jarrett, H. S.; Sleight, a. W.; Ferretti, a. *J. Appl. Phys.* **1977**, *48*, 2463.
(61) Dixit, H.; Saniz, R.; Cottenier, S.; Lamoen, D.; Partoens, B. *J. Phys.: Condens. Matter* **2012**, *24*, 205503.
(62) Whipple, E.; Subbarao, S.; Koffyberg, F. *J. Solid State Chem.* **1980**, *34*, 231−239.
(63) Mohamed, M.; Janowitz, C.; Unger, I.; Manzke, R.; Galazka, Z.; Uecker, R.; Fornari, R.; Weber, J. R.; Varley, J. B.; Van de Walle, C. G. *Appl. Phys. Lett.* **2010**, *97*, 211903.
(64) Tian, W.; Zhi, C.; Zhai, T.; Wang, X.; Liao, M.; Li, S.; Chen, S.; Golberg, D.; Bando, Y. *Nanoscale* **2012**, *4*, 6318−6324.
(65) Lany, S. *Phys. Rev. B* **2013**, *87*, 085112.
(66) Yanagawa, K.; Ohki, Y.; Ueda, N.; Omata, T.; Hashimoto, T.; Kawazoe, H. *Appl. Phys. Lett.* **1993**, *63*, 3335.
(67) Lin, S.; Borgohain, K.; Wei, W. C. J. *J. Am. Ceram. Soc.* **2006**, *89*, 3266−3269.

(68) Dali, S.; Jayachandran, M.; Chockalingam, M. *J. Mater. Sci. Lett.* **1999**, *8*, 915−917.
(69) Yan, C.; Lee, P. *J. Phys. Chem. C* **2009**, *113*, 14135−14139.
(70) Minami, T. *MRS Bull.* **2000**, *25*, 38−44.
(71) Shannon, R. D.; Gillson, J. L.; Bouchard, R. J. *J. Phys. Chem. Solids* **1977**, *38*, 877−881.
(72) Omata, T.; Ueda, N.; Ueda, K.; Kawazoe, H. *Appl. Phys. Lett.* **1994**, *64*, 1077.
(73) Scanlon, D. O. *Phys. Rev. B* **2013**, *87*, 161201.
(74) Badawy, W. A. *Thin Solid Films* **1990**, *186*, 59−72.
(75) Metikos-Hukovic, M.; Lovrecek, B. *Electrochim. Acta* **1980**, *25*, 717−723.
(76) Allen, J. P.; Carey, J. J.; Walsh, A.; Scanlon, D. O.; Watson, G. W. *J. Phys. Chem. C* **2013**, *117*, 14759−14769.
(77) Sleight, A. *Mater. Res. Bull.* **1974**, *9*, 1177−1184.
(78) Schrewelius, N. *Z. Anorg. Allg. Chem.* **1937**, *223*, 241−254.
(79) Shimada, S.; Kodaira, K. *Mater. Res. Bull.* **1986**, *21*, 1495−1501.
(80) Matsushima, S.; Tanizaki, T.; Nakamura, H.; Nonaka, M.; Arai, M. *Chem. Lett.* **2001**, 1010−1011.
(81) Peng, H.; Lany, S. *Phys. Rev. B: Condens. Matter Mater. Phys.* **2012**, *85*, 201202.
(82) Wang, H.; Wang, B.; Li, Q.; Zhu, Z.; Wang, R.; Woo, C. *Phys. Rev. B* **2007**, *75*, 245209.
(83) Bouhemadou, A.; Khenata, R. *Model. Simul. Mater. Sci. Eng.* **2007**, *15*, 787−798.
(84) Medvedeva, J. E. *Europhys. Lett.* **2007**, *78*, 57004.
(85) Mryasov, O.; Freeman, A. *Phys. Rev. B* **2001**, *64*, 2−4.
(86) Burdett, J. K. *Chemical Bonding in Solids*; Oxford University Press: Oxford, 1995.
(87) Gillen, R.; Robertson, J. *J. Phys. Condens. Matter* **2012**, *25*, 165502.
(88) Kato, H.; Kobayashi, H.; Kudo, A. *J. Phys. Chem. B* **2002**, *3*, 12441−12447.
(89) Hoel, C. A.; Mason, T. O.; Gaillard, J.-F.; Poeppelmeier, K. R. *Chem. Mater.* **2010**, *22*, 3569−3579.
(90) Sham, L.; Schlüter, M. *Phys. Rev. Lett.* **1983**, *51*, 1888−1891.
(91) Kawazoe, H.; Yasukawa, M.; Hyodo, H. *Nature* **1997**, 939−942.
(92) Trimarchi, G.; Peng, H.; Im, J.; Freeman, A.; Cloet, V.; Raw, A.; Poeppelmeier, K.; Biswas, K.; Lany, S.; Zunger, A. *Phys. Rev. B* **2011**, *84*, 165116.
(93) Im, J.; Trimarchi, G.; Peng, H.; Freeman, A. J.; Cloet, V.; Raw, A.; Poeppelmeier, K. R. *J. Chem. Phys.* **2013**, *138*, 194703.